SUPPLEMENTAL INFORMATION

SUPPLEMENTAL FIGURES

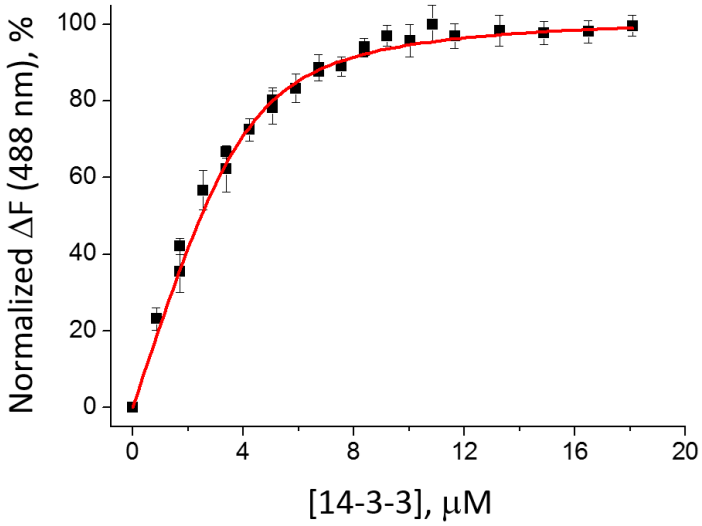

Figure S1 (related to Fig. 2a). Interaction of AEDANS-labeled phosphorylated HSPB6 with 14-3-3σ studied by fluorescence spectroscopy. Titration of 4.2 μM pHSPB6^{AEDANS} solution with 14-3-3σ followed by AEDANS fluorescence intensity (ΔF) at 488 nm (excitation at 336 nm). The ΔF values are expressed as a percentage of ΔF_{max}, the difference of fluorescence at the starting point and at saturation. The curve shows the mean ± SD resulting from three independent experiments.

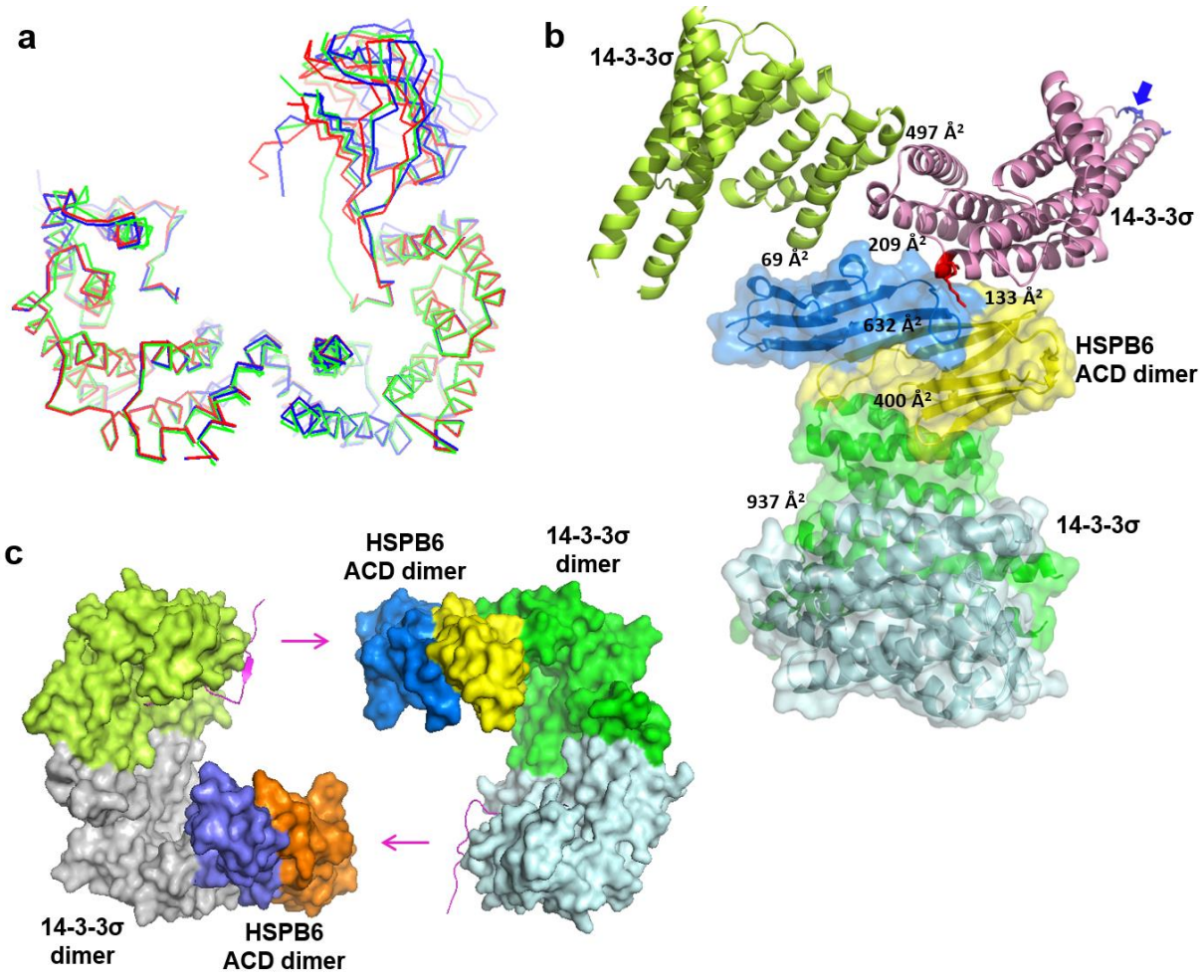

Figure S2 (related to Fig. 3a,b). Structural features of the 14-3-3σ/pHSPB6 crystal structure. **a.** Superposition of the C_α-traces of three symmetry-independent complexes found in the asymmetric unit (red, green and blue respectively). The complexes were superposed by the 14-3-3 dimers. **b.** Crystal contacts made by one heterotetrameric complex (shown as ribbons and surface; the NTDs are omitted) with two 14-3-3 subunits coming from adjacent complexes in the crystal lattice (shown as ribbons). The numbers at the interfaces of the domains show their areas, as determined using PISA (Krissinel and Henrick, 2007). The ACD dimer is wedged in between of three 14-3-3 molecules in the lattice, but the interface with the 14-3-3 chain *within* the heterotetramer is the largest (400Å^2). This packing arrangement remains stable even in the absence of the N-terminal patching, as the heterocomplex of the slightly N-terminally truncated pHSPB6(7-153) produces the same type of crystal lattice. The triple mutation ^{159}AAA^{161} (Clu1) used to improve crystallization of the 14-3-3σ/pHSPB6 complex is highlighted in red on one (pink) 14-3-3 subunit. This mutation is situated in a highly exposed C-terminal end of helix α6. In the crystals, the mutated residues come in contact with the loop connecting strands β5 and β7 of the ACD (coloured marine blue). In addition, blue arrow marks the position of the triple mutation ^{75}AAA^{77} (Clu3) that was used to crystallize the complex with the pHSPB6(13-20) peptide. This mutation resides in a highly exposed loop connecting the helices α3 and α4 of 14-3-3. **c.** A crystal lattice contact made by two 14-3-3σ/pHSPB6 heterotetramers shown as molecular surfaces. The N-terminus of type II (magenta) patches an ACD of the other heterotetramer.

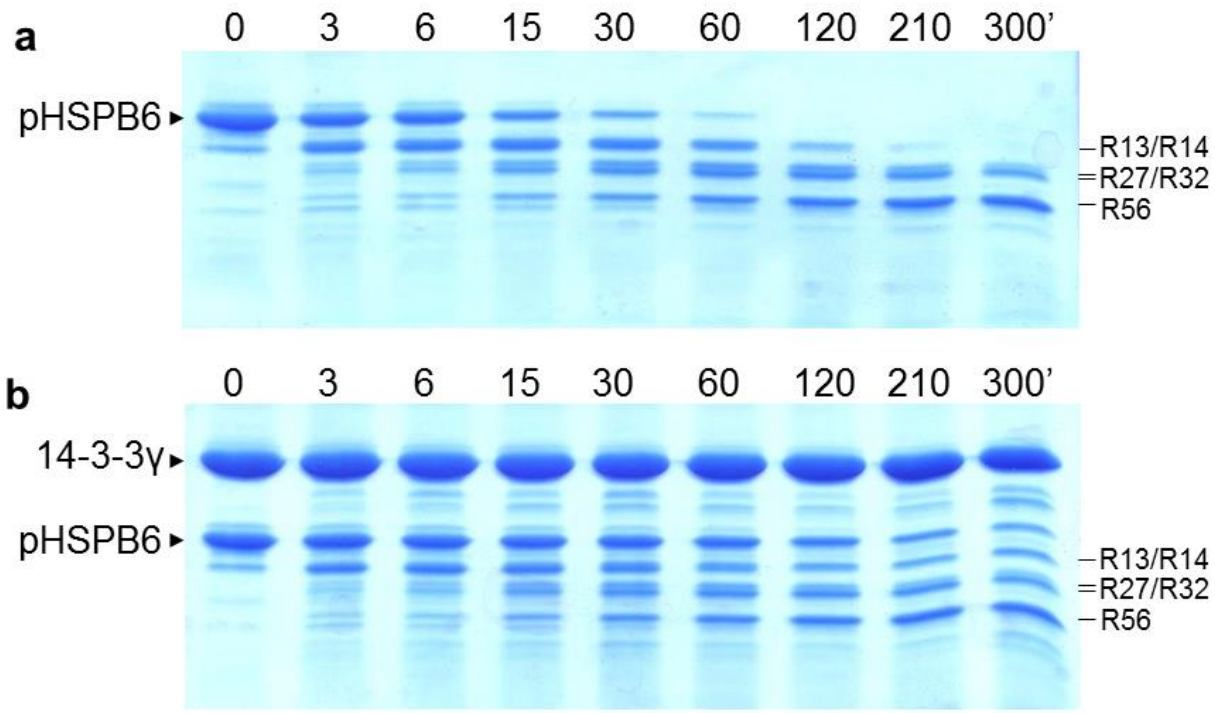

Figure S3 (related to Fig. 4a). The effect of 14-3-3γ on the limited trypsinolysis of HSPB6. Shown is the time course (min) of digestion of pHSPB6 alone (**a**) or the 14-3-3γ/pHSPB6 complex (**b**) at pHSPB6/trypsin weight ratio 1:1500. Although no trypsin was added to the control samples labelled '0', some minor cleavage of pHSPB6 in these samples was still observed, possibly due to cross-contamination. The MS-based identification of the bands as HSPB6 cleavage products at residues R13, R14, R27, R32 and R56 is given to the right. The cleavage of 14-3-3γ alone in a parallel control experiment was not significant, without any cleavage products overlapping with those of HSPB6.

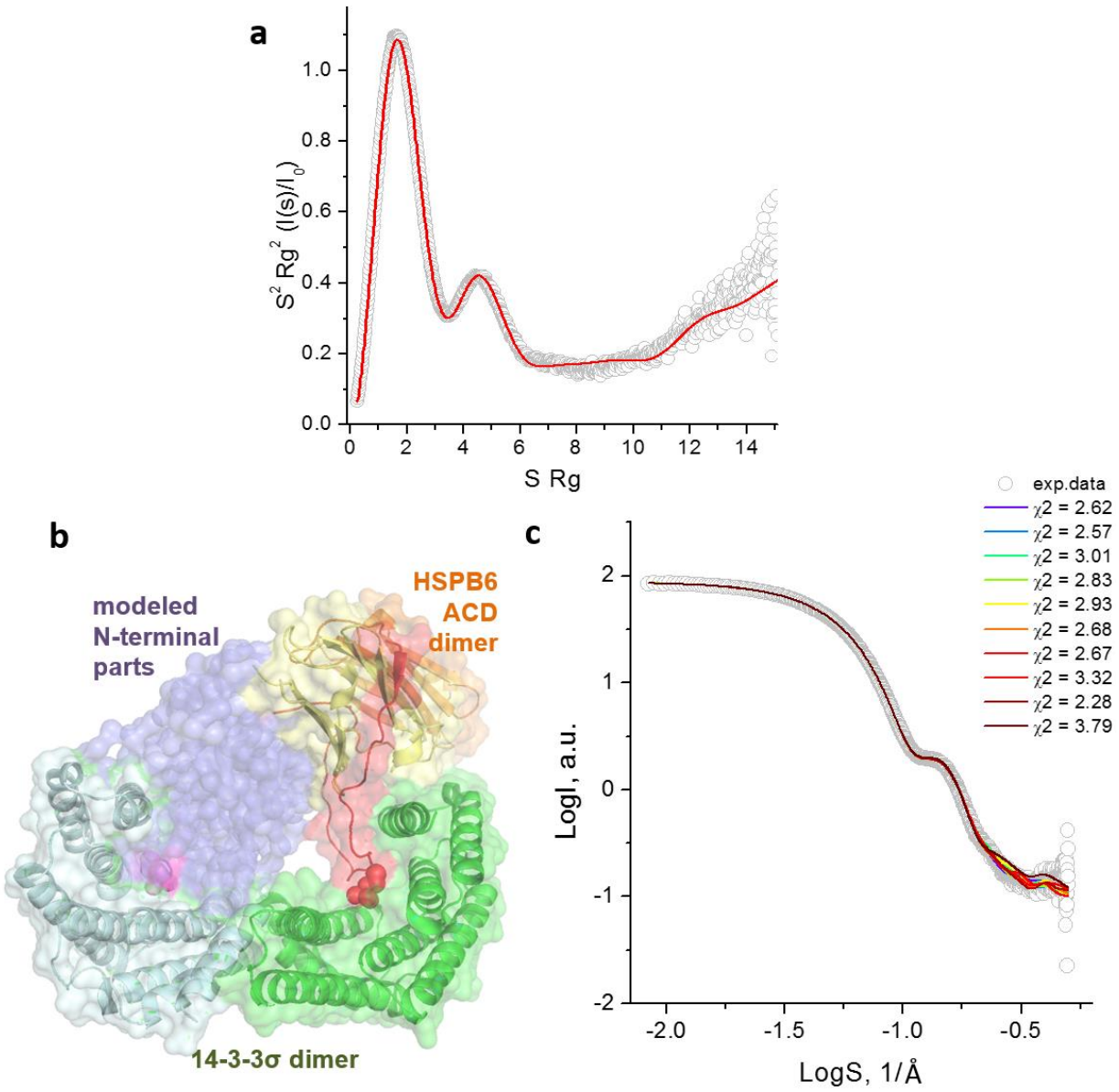

Figure S4 (related to Fig. 4b,c). Modeling of the 14-3-3σ/pHSPB6 structure using solution SAXS data. a. Dimensionless Kratky plot of the data indicating rigidity of the complex in solution. **b.** Superposition of ten independent Coral models built on the basis of the crystallographic structure (shown as ribbons and transparent surface) by addition of the missing NTD regions (shown as space-filling models in violet). **c.** Comparison of the calculated scattering curves from the ten models (lines, rainbow colors) with the experimental SAXS data (circles).

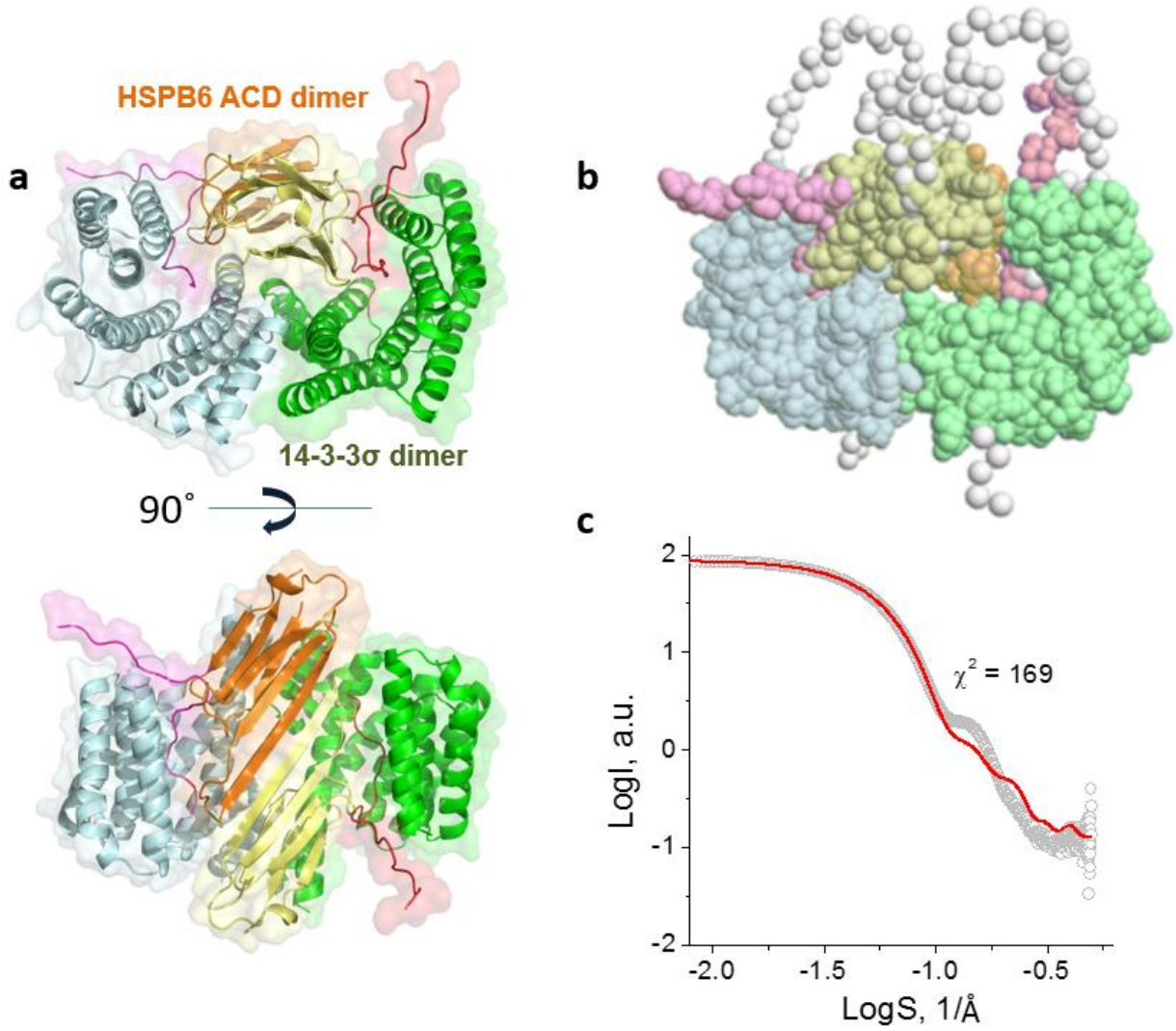

Figure S5 (related to Fig. 4b,c). Alternative 'most compact' symmetrical model of the 14-3-3σ/pHSPB6 complex. a. The model constructed by a rigid-body docking of the ACD dimer into the cavity formed by the 14-3-3 dimer (two orthogonal views). **b.** The same model after Coral-based addition of the missing parts (white spheres). **c.** Fit of the calculated scattering from the latter model to the experimental SAXS data.

SUPPLEMENTAL TABLES

Table S1 (related to Table 1). Crystallization conditions

Complex	14-3-3σ Clu3 (1-231) / pHSPB6 (13-20) peptide	14-3-3σ WT (1-231) / pHSPB6 (11-23) peptide	14-3-3σ Clu1 (1-231) / pHSPB6 (1-149)	14-3-3σ Clu1 (1-231) / pHSPB6 (7-153)	HSPB6 ACD / N-peptide
Precipitant solution	0.1 M Bis-Tris propane (pH 6.5), 0.2 M $NaNO_3$ and 20% PEG 3350	0.1 M HEPES (pH 7.5), 0.2 M $MgCl_2$ and 30% PEG 400	0.1 M HEPES (pH 7.5), 0.2 M LiCl, 17% PEG 6000 and 2 mM DTT	0.1 M HEPES (pH 7.5), 20% PEG 8000 and 2 mM DTT	0.1M Tris-HCl (pH6.5),1.5M ammonium sulfate, 0.1M NaCl
Protein conc. (mg/ml)	11.5	11.5	23	20	15
Temperature (°C)	20	4	4	20	20
Growth time (days)	2-5	5	5	10	14

Table S2 (related to Fig. 5).
Parameters of the three 'druggable' pockets at the 14-3-3σ/pHSPB6 interface

Pocket	Volume	Hydrophobicity	Residues	Polar	Aromatic	Druggability
1	903.9 $Å^3$	-0.24	17	0.41	0.18	**0.78**±0.07
2	344.4 $Å^3$	-0.99	9	0.67	0.11	**0.21**±0.01
3	1990.3 $Å^3$	-0.55	27	0.52	0.15	**0.65**±0.04

Parameters and the druggability score of the three pockets as output by the PockDrug server (http://pockdrug.rpbs.univ-paris-diderot.fr/cgi-bin/index.py?page=Druggability)